Orbital and spin sum rules in x-ray magnetic circular dichroism

W. L. O'Brien
Synchrotron Radiation Center, University of Wisconsin–Madison, 3731 Schneider Drive, Stoughton, Wisconsin 53589

B. P. Tonner
Synchrotron Radiation Center, University of Wisconsin–Madison, 3731 Schneider Drive, Stoughton, Wisconsin 53589
and Department of Physics, University of Wisconsin–Milwaukee, 1900 East Kenwood Boulevard, Milwaukee, Wisconsin 53211
(Received 11 May 1994; revised manuscript received 5 July 1994)

X-ray magnetic circular dichroism (XMCD) in the $L_{2,3}$ absorption spectra of transition metals is a relatively new experimental technique for the investigation of magnetism. XMCD is element specific, giving it obvious advantages over methods which measure averaged magnetic properties. Another potential strength of XMCD is the separate quantitative measurement of $\langle L_Z \rangle$ and $\langle S_Z \rangle$ through application of dichroism sum rules. In this paper we present the results from a set of experiments designed to test the applicability of the dichroism sum rules to XMCD spectra measured by total electron yield. We find that with proper experimental control of angle of incidence, degree of polarization and film thickness, the total electron yield measurement of absorption spectra is accurate to within 5%. The uncertainties involved in applying the dichroism sum rules are discussed in detail, including possible effects of diffuse magnetic moments which are known to exist in Fe, Co, and Ni. The magnitude of these uncertainties makes it difficult to obtain absolute values of $\langle L_Z \rangle$ and $\langle S_Z \rangle$, however, the dichroism sum rules are shown to be qualitatively accurate and therefore capable of measuring changes in $\langle L_Z \rangle$ and $\langle S_Z \rangle$.

I. INTRODUCTION

Magnetic circular dichroism in the $L_{2,3}$ absorption spectra of the magnetically interesting $3d$ transition metals is readily measurable using synchrotron radiation. These x-ray magnetic circular dichroism (XMCD) measurements have become widely used for the study of magnetism since the results by Chen *et al.*[1] To date, $L_{2,3}$ XMCD from the first row transition-metal elements has been reported for V,[2,3] Cr,[4] Mn,[5,6] Fe,[7] Co,[8,9] Ni,[1,10,11] and Cu.[12] The core holes involved in the $L_{2,3}$ XMCD process make the measurement element specific, giving it obvious advantages over methods which measure averaged magnetic properties. Recent theoretical analysis of the $2p$-$3d$ transitions in atoms finds that ground-state expectation values of $\langle L_Z \rangle$ and $\langle S_Z \rangle$ can be derived from the dichroism spectra.[13,14] If these predictions are realized as well for solids, XMCD will become one of the most versatile and useful techniques for the study of magnetic materials.

The theoretical understanding of XMCD can be traced to work by Erskine and Stern[15] who showed that the ratio of the integrated dichroism intensity at the L_3 and L_2 edges, R_M, is equal to -1 for a simple atomic model. Early measurements on Ni by Chen *et al.*[1,11] found values of R_M much different than -1. Smith *et al.*[7] showed that agreement with experiment could be substantially improved for Ni by including the spin-orbit interaction between the ground-state valence d electrons in the calculation. However, this analysis failed when applied to Fe, leading Smith *et al.*[7] to argue that a single-particle calculation could not explain XMCD in the $3d$ transition metals. More recently, Thole *et al.*[13] and Carra *et al.*[14] have derived sum rules which relate the integrated intensity of the dichroism signal at the L_3 and L_2 edges to $\langle L_Z \rangle$ and $\langle S_Z \rangle$ for atoms. These calculations include many-body effects, but treat only the $2p \rightarrow 3d$ transitions and therefore cannot account for effects in the solid phase such as *spd* wave mixing, or the overlap of the *sp* band and the *d* band.

Application of the atomic dichroism sum rules to solids is still controversial. Wu, Wang, and Freeman,[16] using local-density energy-band calculations, showed that the $\langle L_Z \rangle$ sum rule was accurate to within 10%, if effects of band hybridization could be accounted for experimentally. These calculations ignore many-body effects and produce absorption and dichroism spectra that differ noticeably from experimental line shapes. Wu, Wang, and Freeman[17] also argue that the magnetic dipole term, $\langle T_Z \rangle$, which Carra *et al.*[14] assumed to negligible, can be important and affect the $\langle S_Z \rangle$ sum rule for solids lacking cubic symmetry. Another potential uncertainty in the application of the sum rules to solids is the presence of *s*-wave diffuse magnetic moments[18,19] which are known to exist in Fe, Co, and Ni.

In addition to the theoretical ambiguities, there are a number of experimental difficulties involved in the application of the dichroism sum rules. Most importantly, the precise relationship between the absolute photoabsorption cross section and the detected signal must be well understood. X-ray-absorption measurements are typically made by monitoring the total electron yield $Y(\hbar\omega)$ or the fluorescence yield. Absorption spectra, $\sigma(\hbar\omega)$, are typically determined from $Y(\hbar\omega)$ using the relationship $Y(\hbar\omega) \propto \hbar\omega\sigma(\hbar\omega)$. This simple relationship between absorption and total electron yield is not always valid at the $L_{2,3}$ absorption edges of $3d$ transition metals,[20] and "saturation effects" can introduce large errors

in the dichroism measurement. In an investigation of the dichroism from V, Cr, Mn, Fe, Co, and Ni, O'Brien *et al.*[3] have pointed out other experimental difficulties in applying the sum rules. These include the presence of a dichroism signal between the L_3 and L_2 white lines and an overlap of the L_3 and L_2 spectra.

In this paper we report on a series of experiments designed to produce high-quality XMCD spectra in an attempt to determine whether the dichroism sum rules are valid for solids. To do this we measure the dichroism in the $L_{2,3}$ absorption spectra of thin films of 3*d* transition metals. The details of these measurements are described in Sec. II. In Sec. III we study the saturation effect on the total electron yield measurement and identify appropriate experimental conditions for measuring absorption cross sections and dichroism by total electron yield. In Sec. IV we examine the details of the XMCD spectra and show how diffuse magnetic moments may account for previously unexplained features in the dichroism spectra of Co and Ni. In Sec. V we test $\langle L_Z \rangle$ and $\langle S_Z \rangle$ dichroism sum rules on high-quality Fe, Co, and Ni XMCD spectra.

To aid in the discussion that follows, we make the following definitions. The magnetic dichroism, $\sigma_M = (\sigma_+ - \sigma_-)$, is the difference between the absorption spectra with the photon spin parallel (σ_+) and antiparallel (σ_-) to the sample magnetization **M**. The average of the two spectra, $(\sigma_+ + \sigma_-)/2$, is in most circumstances considered to be identical to the absorption cross section for photon spin orthogonal to the sample magnetization σ_0. In the work presented below we directly measure the total electron yield, $Y(\hbar\omega)$, rather than the absorption cross section $\sigma(\hbar\omega)$. We therefore also define Y_+, Y_-, and Y_0 in a manner consistent with the definitions of σ_+ σ_-, and σ_0. The intensity and sign of σ_M depends on the relative orientation of **M** and the photon spin, **Σ**, that is $\sigma_M \sim \mathbf{\Sigma}\cdot\mathbf{M}$. This is an important property of XMCD, since it allows the direction of **M** to be determined. XMCD spectra are presented normalized to σ_0 at the L_3 peak, $\sigma_M(\hbar\omega)/\sigma_0(L_3)$. The relative degree of magnetic ordering is discussed in terms of the absolute value of $\sigma_M(\hbar\omega)/\sigma_0(L_3)$ measured at the L_3 edge, $|\sigma_M(L_3)/\sigma_0(L_3)|$. The integrated intensities of the L_3 and L_2 peaks in the σ_M spectrum are important quantities related to $\langle L_Z \rangle$ and $\langle S_Z \rangle$ by the dichroism sum rules. We define these as ΔA_{L_3} and ΔA_{L_2}, respectively, and also define the ratio $R_M = \Delta A_{L_3}/\Delta A_{L_2}$.

II. EXPERIMENTAL APPARATUS

The measurements were performed on the 10-m toroidal grating monochromator located at the Synchrotron Radiation Center (SRC) of the University of Wisconsin. The beamline is equipped with a water-cooled copper aperture which allows the selection of either linear, left-handed or right-handed elliptically polarized photons in the energy range 200–900 eV. Right-handed or left-handed elliptically polarized photons are selected by blocking out the bottom or top portion of the photon beam, respectively. The degree of circular polarization, obtained by blocking off all but the top or bottom 10% of the photon beam, has been calculated to be 85±5% over the range of the monochromator.[21]

Thin films of Fe, Co, and Ni were grown *in situ* on a Cu(001) substrate. Fe, Co, and Ni were evaporated at a rate of 1-ML/min by restively heating pure wires. The pressure during evaporation was below 1×10^{-9} Torr. The Cu substrate was cleaned by argon-ion bombardment and annealing. The substrate and film purity was confirmed with photoemission spectroscopy. Low-energy electron diffraction was used to determine substrate and film order. The film thickness was monitored by a quartz-crystal microbalance at the sample position. The calibration of the microbalance was checked using two methods. First, photoemission intensities of substrate and overlayer were measured and corrected to absolute intensities using atomic cross sections. Second, a similar procedure was applied to the substrate and overlayer x-ray-absorption intensity. The agreement between film thickness measurements indicates that our reported film thicknesses are accurate to within 20%. This accuracy has also been confirmed by comparing our magnetization vs film thickness results for Fe, Co, and Ni growth on Cu(001) to previously published results.

After growth, the samples were magnetized *in situ* by a 2-kG electromagnet with the field either perpendicular to the surface or in-plane along any chosen axis. Absorption measurements could be made with the photon angle of incidence, θ, varying between −70° and 70°, relative to the surface normal. For in-plane magnetization, absorption spectra are taken at θ and $-\theta$ without remagnetizing the sample and without changing the photon polarization, see Fig. 1. This is equivalent to changing the sample magnetization and allows for complete control of $\mathbf{\Sigma}\cdot\mathbf{M}\sim\cos\phi$, see Fig. 1 where ϕ is the angle between **Σ** and **M**. In this manner the direction of **M** can be determined. For perpendicular magnetization the photon beam is fixed at normal incidence and spectra are taken with $\phi = 0°$ and 180°, by either remagnetizing the sample or changing the photon polarization.

This measurement technique has been checked using left-handed and right-handed circularly polarized photons. In Fig. 2 we show two Fe σ_M spectra obtained from a 15-ML film of Fe grown on Cu(001). The film was magnetized in-plane along the [110] direction. To gen-

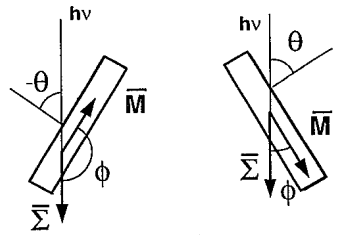

FIG. 1. Experimental arrangement for measuring σ_-, left, and σ_+, right, for samples magnetized in-plane. The angle between the photon spin vector, **Σ**, and the sample magnetization, **M**, is ϕ and the photon angle of incidence with respect to the surface normal is θ. For in-plane magnetization, $\theta = 90 - \phi$.

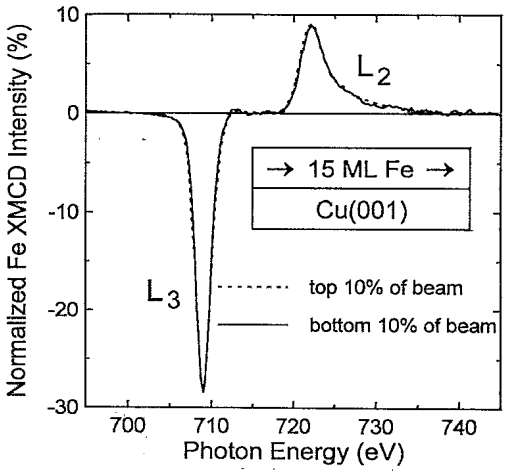

FIG. 2. Comparison of σ_M spectra from a 15-ML-Fe film using (separately) right- or left-handed circular polarization, obtained using light above or below the orbital plane. Each polarization was used to measure σ_- and σ_+. The two different helicity measurements are virtually indistinguishable.

erate each Fe σ_M spectra, absorption measurements were taken at $\theta=45$ and -45 degrees. For one σ_M spectrum the top 10% of the photon beam was used, for the other the bottom 10% was used. These two σ_M spectra are essentially identical. The spectrum obtained using the bottom of the photon beam has been shifted 0.2 eV toward higher photon energy to align the L_3 peaks. This most likely is the result of the different optical paths taken by x-rays above and below the storage ring orbital plane, resulting in a small energy shift. Because of this problem we typically make our dichroism measurements by keeping the photon polarization constant and changing the sample magnetization by rotating the sample.

All total electron yield measurements were made on the remanent sample magnetization at room temperature in a chamber with background pressure of 6×10^{-11} Torr. The total electron yield spectra, $Y(\hbar\omega)$, were obtained by measuring the sample drain current. The experimental conditions in which $Y(\hbar\omega)\propto\hbar\omega\sigma(\hbar\omega)$ is a valid approximation are considered in detail in Sec. III. The yield spectra were corrected for the incident photon flux on the sample and the $\hbar\omega$ dependence using a Au photodiode current, normalized according to tabulated Au photoyield.[22] This result was confirmed using a Cu diode. A linear background was subtracted from the spectra to remove contributions from the substrate.

III. SATURATION IN TOTAL ELECTRON YIELD

In this section we show that it is important to consider saturation effects when determining the absorption cross section from total electron yield. It is commonly assumed that there is a simple relationship between the total electron yield, $Y(\hbar\omega)$, and the absorption cross section, $\sigma(\hbar\omega)$,

$$Y_i(\hbar\omega)\propto\hbar\omega\sigma_i(\hbar\omega)\ , \tag{1}$$

where $i=0,+$ or $-$. As we show below, this approximation is not always valid. For example, at close to zero degrees grazing incidence all the photons are absorbed near the surface and the total electron yield is proportional to the incident flux, independent of $\sigma(\hbar\omega)$. While more accurate relationships between $Y_i(\hbar\omega)$ and $\sigma_i(\hbar\omega)$ can easily be derived, they include parameters which are not precisely known. The uncertainties in these parameters could result in large errors in the dichroism measurements. We therefore take the following approach to obtain $\sigma(\hbar\omega)$ from our total electron yield measurements. First, we make a more complete model of the total electron yield process for thin-film and multilayer systems. We then compare angular-dependent experimental results to this model. After verifying our model we are then able to identify experimental conditions where (1) is a good approximation.

A more complete expression for $Y_i(\hbar\omega)$ should consider the angle of incidence of the photon beam, the film thickness, the alignment of $\mathbf{M}$ and $\mathbf{\Sigma}$, and the secondary electron escape depth. For a film that is laterally homogeneous, and varies in atomic density with depth z, we find

$$Y_i(\hbar\omega)=J_0(\hbar\omega)N(\hbar\omega)\int_0^d\frac{\sigma_i(\hbar\omega,z)\rho(z)}{\cos\theta}\exp\left[-\int_0^z\left[\frac{\sigma_i(\hbar\omega,z')\rho(z')}{\cos\theta}+\frac{1}{\lambda_e(z')}\right]dz'\right]dz \tag{2}$$

with

$$\sigma_\pm(\hbar\omega)=\sigma_0(\hbar\omega)-\frac{\sigma_d(\hbar\omega)P}{2}\cos\phi\ . \tag{3}$$

Here $J_0(\hbar\omega)$ is the incident photon flux, $N(\hbar\omega)$ is the number of secondary electrons produced per photon which run in the direction of the surface, d is the film thickness, P is the degree of circular polarization, and ρ is the atomic density. The detection depth for total electron yield is assumed to be the effective escape depth of secondary electrons, λ_e. We have previously reported[8] an experimental value of 20 Å for λ_e. There are two angles which are important in this analysis, see Fig. 1. The photon angle of incidence, θ, is important for determining the effects of saturation. The angle between $\mathbf{M}$ and $\mathbf{\Sigma}$, ϕ, determines the magnitude of σ_+ and σ_-. In (3), σ_d is the limiting value of σ_M, for $P=1$ and

$\phi=0$. Thus $\sigma_{\pm}(\hbar\omega)$ depends on ϕ, while $Y_{\pm}(\hbar\omega)$ depends on both ϕ and θ.

For a well-ordered multilayer system consisting of d_1 Å of element 1 on top of d_2-d_1 Å of element 2, etc.,

$$Y_i(\hbar\omega)=\frac{J_0(\hbar\omega)N(\hbar\omega)}{\cos\theta}\left\{\int_0^{d_1}\rho_1\sigma_{i,1}(\hbar\omega)\exp\left[-z\left[\frac{\rho_1\sigma_{i,1}(\hbar\omega)}{\cos\theta}+\frac{1}{\lambda_e}\right]\right]dz + \left[1-\exp\left[\frac{-d_1\rho_1\sigma_{i,1}(\hbar\omega)}{\cos\theta}\right]\right]\int_{d_1}^{d_2}\rho_2\sigma_{i,2}(\hbar\omega)\exp\left[-z\left[\frac{\rho_2\sigma_{i,2}(\hbar\omega)}{\cos\theta}+\frac{1}{\lambda_e}\right]\right]dz+\ldots\right\} \quad (4)$$

assuming that λ_e is constant. For a thin film consisting of a single element (4) reduces to

$$Y_i(\hbar\omega)=\frac{J_0(\hbar\omega)N(\hbar\omega)\sigma_i(\hbar\omega)\rho}{\cos\theta}\times\int_0^d\exp\left[-d\left[\frac{1}{\lambda_e}+\frac{\sigma_i(\hbar\omega)\rho}{\cos\theta}\right]\right]dz\ . \quad (5)$$

The secondary electron kinetic-energy distribution is typically peaked near a kinetic energy of 5 eV so that for $\hbar\omega\gg5$ eV the approximation $N(\hbar\omega)\propto\hbar\omega$ is commonly used. Thus,

$$Y_i(\hbar\omega)\propto\frac{\hbar\omega\sigma_i(\hbar\omega)}{\cos\theta}\left[\frac{1}{1/\lambda_e+\sigma_i(\hbar\omega)\rho/\cos\theta}\right]\times\left\{1-\exp\left[-d\left[\frac{1}{\lambda_e}+\frac{\sigma_i(\hbar\omega)\rho}{\cos\theta}\right]\right]\right\}, \quad (6)$$

and it is apparent that (1) is a valid approximation to (6) when $\lambda_e\ll\cos\theta/\sigma(\hbar\omega)\rho$. In the limit of $\cos\theta/\sigma\to0$, (6) reduces to $Y_i(\hbar\omega)\propto\hbar\omega/\rho$, which is independent of the sample cross section. This is the saturation effect in total electron yield. At large angles of incidence and for photon energies near a strong absorption edge (such as the L_3 and L_2 peaks) we expect the approximation (1) to fail. Approximation (1) is also valid for very thin films,

$$d\ll\left[\frac{1}{\lambda_e}+\frac{\sigma_i(\hbar\omega)\rho}{\cos\theta}\right]^{-1}. \quad (7)$$

In order to determine the experimental conditions where (1) is a good approximation to (6) we have measured the Fe yield spectra Y_+ and Y_- from a 500-Å-thick Fe film grown on Cu(001) as a function of θ. The film was magnetized in-plane along the [110] direction. XMCD spectra were obtained from these measurements by assuming that the approximation (1) is valid. These σ_M spectra are shown in Fig. 3 where each has been normalized to σ_0 at the L_3 peak. These spectra have also been corrected for incomplete photon polarization, assuming $P=0.85$. The intensity of the σ_m signal qualitatively follows $\boldsymbol{\Sigma}\cdot\mathbf{M}\sim\cos\phi$.

For a quantitative investigation of these results we plot $|\sigma_M(L_3)/\sigma_0(L_3)|$ vs ϕ and θ in Fig. 4(a) and R_M vs ϕ and θ in Fig. 4(b). For in-plane magnetization $\theta=(90-\phi)$. The dotted lines in Fig. 4 show the expected behavior of $|\sigma_M(L_3)/\sigma_0(L_3)|$ and R_M, $|\sigma_M(L_3)/\sigma_0(L_3)|\propto\cos\phi$ and a constant R_M. The data were fitted at small values of θ, where $Y(\hbar\omega)\propto\hbar\omega\sigma(\hbar\omega)$ is more accurate. Both the normalized XMCD intensity and R_M divert from this fit above $\theta=50$ degrees. The approximation (1) gives values of $|\sigma_M(L_3)/\sigma_0(L_3)|$ and R_M which are valid to within 5% for $\theta<50$ degrees for thick Fe films and for this choice of polarization, 0.85. For larger values of θ, errors in excess of 10% are possible.

We now wish to see if the deviations between the experimental results obtained assuming (1) and the expected results can be explained by saturation (6). Before we can do this, values of $\sigma_0(\hbar\omega)$ and $\sigma_d(\hbar\omega)$ must be known. Absolute measurements of $\sigma(\hbar\omega)$ are very difficult so we choose the following approach. The approximation $Y_0(\hbar\omega)\propto\hbar\omega\sigma_0(\hbar\omega)$ should be valid for very thin films at normal incidence. We therefore start with the yield spectrum of a 2-ML film taken at normal incidence and use approximation (1) to determine the relative cross section as a function of energy, $\sigma_0^{\rm rel}(\hbar\omega)$. The absolute cross section, $\sigma_0(\hbar\omega)$, is determined by measuring the jump at the L_3 edge in the yield spectra for a very thick film and setting the absorption cross section just before the L_3 edge

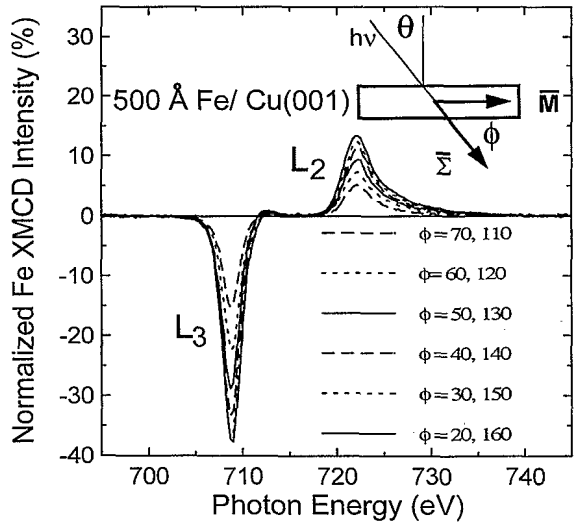

FIG. 3. Normalized Fe σ_M spectra obtained at different angle of incidence, θ, from a 500-Å film magnetized in-plane. Spectra have been multiplied by 1.18 to account for incomplete photon polarization.

to the atomic value.[22] In this manner $\sigma_0(\hbar\omega)$ just before the L_3 edge and at the peak of the L_3 edge for Fe is 0.2 and 2.6 Mb/atom, respectively. For Co the values are 0.2 and 2.0 Mb/atom and for Ni 0.2 and 1.5 Mb/atom. To determine $\sigma_d(\hbar\omega)$ we use a measured $\sigma_M(\hbar\omega,\phi=60°)$ spectrum and set $\sigma_d(\hbar\omega)=\sigma_M(\hbar\omega,\phi=60°)/(P\cos 60°)$. $\sigma_+(\hbar\omega)$ and $\sigma_-(\hbar\omega)$ are then determined from (3).

We can now show that the deviations between the experimental results obtained assuming (1) and the expected results in Fig. 4 can be explained by saturation. To do this we generate the $Y_\pm(\hbar\omega)$ spectra for different photon angles of incidence using (6), and the approximations for $\sigma_\pm(\hbar\omega)$. From these spectra we obtain $|\sigma_M(L_3)/\sigma_0(L_3)|$ and R_M for different values of θ using approximation (1). The solid lines in Fig. 4(a) and Fig. 4(b) are the results of these calculations which fit the data quite well, showing the validity of (6). The values for both $|\sigma_M(L_3)/\sigma_0(L_3)|$ and R_M vs θ determined by this approach are parameterless. Approximation (1) is valid to within 5% for values of $\theta<50°$ degrees and the deviations for $\theta>50$ are due to saturation in total electron yield as described by (6). The good agreement between experiment and theory gives us confidence in our theoretical modeling using (6) and allows us to determine the experimental conditions in which (1) is a good approximation.

As a test, we measure the angular dependence of R_M and $|\sigma_M(L_3)/\sigma_0(L_3)|$ of a 10-ML film of fcc Co grown on Cu(001),[23] Fig. 5. A 10-ML film was chosen to be in the regime of validity of (1). Furthermore the degree of circular polarization was reduced to 70% to lower the maximum value of $\sigma_-(\hbar\omega)$, which also should increase the validity of (1). The experimental results in Fig. 5 were obtained from yield spectra assuming (1) and are

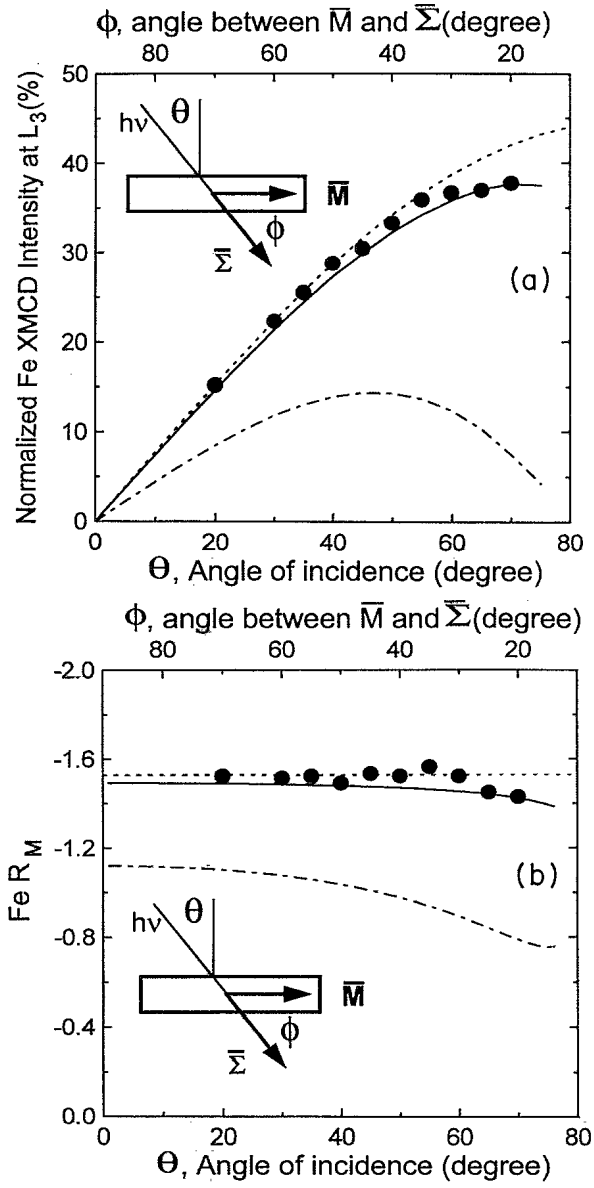

FIG. 4. (a) Normalized Fe σ_M intensity at the L_3 edge vs θ and ϕ obtained from results in Fig. 3. For $\theta<50$ degrees the results agree well with the approximation $Y(\hbar\omega)\propto\hbar\omega\sigma(\hbar\omega)$, dotted line. Errors $>10\%$ result from the approximation $Y(\hbar\omega)\propto\hbar\omega\sigma(\hbar\omega)$ for larger θ. The deviations for $\theta>50°$ are explained by saturation effects in the total electron yield measurement, solid line. The predicted dependence of $|\sigma_M(L_3)/\sigma_0(L_3)|$ using fluorescence yield is also shown, dash-dotted line. All values have been multiplied by 1.18 to account for incomplete photon polarization. (b) Values of R_M vs θ and ϕ obtained from results in Fig. 3. For $\theta<55$ degrees the results agree with the approximation $Y(\hbar\omega)\propto\hbar\omega\sigma(\hbar\omega)$, dotted line. The deviations for $\theta>55$ are explained by saturation in the total electron yield measurement, solid line. The predicted dependence of R_M using fluorescence yield is also shown, dash-dotted line.

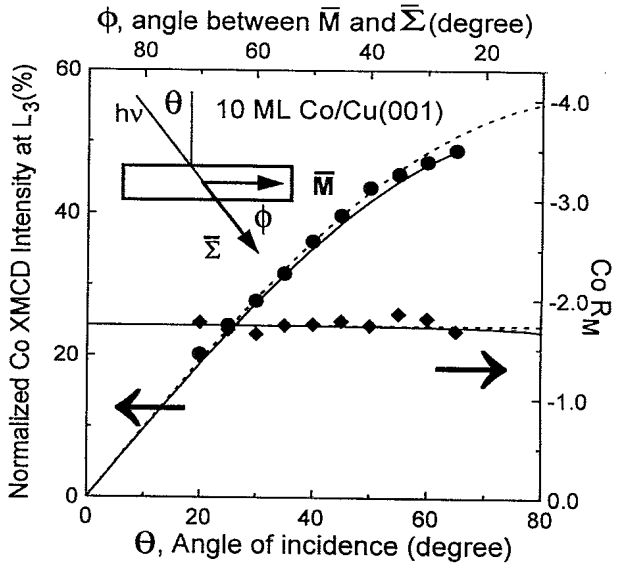

FIG. 5. Normalized Co σ_M intensity at the L_3 edge, circles, and values of R_M, diamonds, vs θ and ϕ obtained from a 10-ML-Co film magnetized in-plane. Results are fitted assuming $Y(\hbar\omega)\propto\hbar\omega\sigma(\hbar\omega)$, dotted line. Deviations due to saturation in the total electron yield measurement are shown by the solid line. For this film thickness and degree of circular polarization, 0.7, the approximation $Y(\hbar\omega)\propto\hbar\omega\sigma(\hbar\omega)$ is valid to within 5% for $\theta<65$ degrees. Normalized Co σ_M intensities have been multiplied by 1.43 to account for incomplete photon polarization.

compared to $|\sigma_M(L_3)/\sigma_0(L_3)| \propto \cos\phi$ and a constant R_M, dashed lines, and values of $|\sigma_M(L_3)/\sigma_0(L_3)|$ and R_M corrected for saturation assuming (6), solid lines. The errors due to approximation (1) for both $|\sigma_M(L_3)/\sigma_0(L_3)|$ and R_M are less than 5% for values of $\theta \leq 65$. The results in Figs. 4 and 5 show that by properly selecting experimental conditions the approximation (1) can be made valid to within $<5\%$. In cases where it is not possible to properly select experimental conditions (6) can be used to adjust experimental values of $|\sigma_M(L_3)/\sigma_0(L_3)|$ and R_M obtained by total electron yield measurements.

To this point we have only discussed the implications of using total electron yield to measure the sample absorption. It is important to also consider other means of measuring the sample absorption. Fluorescence detection, using the $L_{2,3}$ soft x-ray emission intensity to monitor absorption, is one alternative technique. This method is not sensitive to sample charging or magnetic fields. However, the mean free path of detection in these experiments is very large. In Fig. 4 we have modeled the expected results of $|\sigma_M(L_3)/\sigma_0(L_3)|$ and R_M for fluorescence detection, dash-dot lines, assuming the absorption cross section to be proportional to the fluorescence yield. For these calculations we assumed a detector at normal incidence and a mean free path of detection derived from the pre-L_3 edge cross section, 6000 Å.[22] Due to the long mean free path of detection, measurements of $|\sigma_M(L_3)/\sigma_0(L_3)|$ and R_M using fluorescence are not valid for samples this thick. Additional problems with fluorescence measurements are the difference in the mean free path of the emitted L_2 and L_3 photons (due to self-absorption) and dichroism in the soft-x-ray-emission intensity.[24]

Other methods of measuring absorption are the partial electron yield and transmission techniques. Partial electron yield detection, using Auger electrons, should have a mean free path of detection equal to or smaller than total electron yield measurements. This suggests that the absorption cross section should be proportional to the Auger yield over a similar range of experimental conditions as found for the validity of (1). For a few magnetic thin-film systems we have used both the Auger yield and total electron yield to measure XMCD. These results were similar, however, the counting rate for the Auger yield spectra was much lower. Other problems associated with Auger yield detection are the possibility of stray fields from the magnetized sample affecting the measurement.

X-ray transmission measurements are attractive, since $\sigma_+(\hbar\omega)$ and $\sigma_-(\hbar\omega)$ can be measured directly. This method is, however, limited due to experimental constraints such as the necessity of using free standing films of appropriate thickness or films grown on transparent substrates.

A combination of measurement techniques which probe different depths will be useful in the study of magnetic properties of thin films and multilayers. Experiments of this type may allow the magnetic properties of surfaces and interfaces to be distinguished from bulk magnetic properties. For a valid comparison of dichroism effects using different measurement techniques, Eq. (6), and its analogs for other absorption measurements, will be necessary. The results presented in Figs. 4 and 5, which show good agreement between (6) and experiment, prove that such experiments can be interpreted with a reasonable degree of certainty.

IV. DIFFUSE MAGNETIC MOMENTS

In this section we examine the details of high-quality Fe, Co, and Ni XMCD spectra and show that weak features in the Co and Ni spectra may be due to diffuse magnetic moments. In Fig. 6 we show the XMCD spectra of Ni, Co, and Fe, normalized to constant L_3 peak height. These spectra were obtained under conditions where $Y(\hbar\omega) \propto \hbar\omega\sigma(\hbar\omega)$ is valid to within $<5\%$. Details of the low-intensity features in these spectra are shown in Fig. 7 on an expanded scale defined by the dashed lines in Fig. 6. The samples used were bcc Fe, fcc Co, and fcc Ni thin films of 25, 15, and 20 ML thick, respectively, grown on Cu(001). The Fe and Co films were magnetized in plane and the Ni film was magnetized perpendicular to the surface.

There is a shoulder on the high-energy side of the Ni L_3 peak, labeled B in Fig. 6, and then a small constant negative intensity up to the beginning of the L_2 edge. The shoulder B, is due to a d^8 initial-state configuration, while the main L_3 peak is due to a d^9 initial state configuration.[25,26] The constant negative intensity between B and the L_2 edge is present in other published spectra,[7,11] but its origin has not been discussed. This feature is not present in relativistic tight-binding calcula-

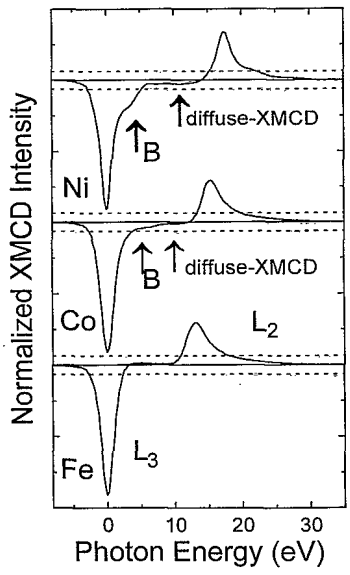

FIG. 6. Fe, Co, and Ni XMCD spectra shown normalized to constant L_3 peak height. The features labeled B are due to multiple initial-state configurations. The constant negative intensity between B and the L_2 peak in the Ni and Co spectra is due to diffuse magnetism.

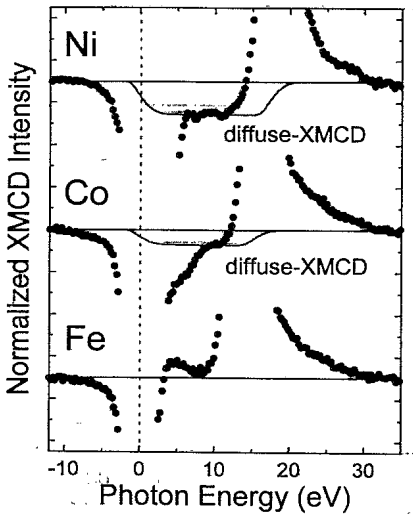

FIG. 7. Same spectra shown in Fig. 6 on an expanded scale defined by the dashed lines in Fig. 6 showing XMCD due to diffuse magnetism in the Ni and Co spectra.

tions which considered $2p \rightarrow 3d$ excitations only.[7]

The Co XMCD spectrum is similar to the Ni XMCD spectrum. There is a negative shoulder on the high-energy side of the L_3 peak and a small constant negative intensity up to the beginning of the L_2 edge. Both of these smaller weak features are present in published spectra for hcp Co (Ref. 9) but the identity of neither of them has been discussed. We assume that the shoulder is due to an additional initial-state configuration as for Ni and therefore have labeled it B in Fig. 6.

The details of the Fe XMCD spectrum are different than the Ni and Co spectra. There is a small positive intensity shoulder above the L_3 edge and then the intensity approaches zero before the L_2 peak. This is part of a trend in the XMCD spectra of $3d$ transition metals where the L_3 peak has a negative intensity shoulder for Ni and Co and an increasingly positive intensity shoulder for Fe, Mn, Cr, and V.[3] While the negative intensity shoulders in the Ni and Co spectra can be explained by multiple initial-state configurations, the positive shoulders in the Mn and Cr spectra are present in calculations for Mn d^5 and Cr d^4 states.[27]

The XMCD intensities between the L_2 and L_3 edges must be understood before the dichroism sum rules can be tested. One possible identity for the negative Co and Ni XMCD intensities between the shoulder B and the L_2 edge is diffuse magnetic moments. Polarized neutron-diffraction studies on Fe, Co, and Ni have revealed the existence of a diffuse background magnetism with sign opposite to the sample magnetization.[18] This background magnetism was assumed to be caused by $4s$ electrons, whose spin is oppositely polarized to the $3d$ electrons. Recent band-structure calculations on Fe, Co, and Ni also predict negative diffuse magnetism due to the sp-projected and interstitial moments.[19] The results from these calculations and the neutron-scattering experiments are summarized in Table I. Since $L_{2,3}$ absorption spectra

TABLE I. Diffuse moment, μ_{diff} and ratio of diffuse moment to total moment, $\mu_{\text{diff}}(\%)$, for Ni, Co, and Fe determined by calculation and by neutron diffraction (ND). Values are given in μ_B/atom.

	Ni		Co		Fe	
	Theory[a]	ND[b]	Theory[a]	ND[b]	Theory[a]	ND[b]
μ_{diff}	−0.04	−0.105	−0.07	−0.28	−0.04	−0.21
$\mu_{\text{diff}}(\%)$	−7%	−17%	−4%	−16%	−2%	−10%

[a]Reference 19.
[b]Reference 18.

are sensitive to both s- and d-electron levels, it is expected that diffuse magnetism will affect the XMCD spectra.

To predict the effects of diffuse magnetism on the XMCD spectra we use a simple atomic model similar to that used by Erskine and Stern.[15] We assume that the empty d levels have minority-spin character ($\downarrow$) and that the empty s levels have majority-spin character ($\uparrow$), due to the opposite orientation of the s and d levels. No spin-orbit coupling is included in the d levels. The calculated XMCD intensities for transitions into s and $3d$ levels are given in Table II for both L_3 and L_2 where[28]

$$A \equiv |\langle Y_{2\pm2}|x \pm iy|Y_{1\pm1}\rangle|^2 = \tfrac{4}{5} ,$$

$$C \equiv |\langle Y_{20}|x \mp iy|Y_{1\pm1}\rangle|^2 = \tfrac{2}{15} ,$$

$$D \equiv |\langle Y_{00}|x \mp iy|Y_{1\pm1}\rangle|^2 = \tfrac{2}{3} .$$

This simple model predicts an R_m of -1 for excitation into both the $3d(\downarrow)$ and $s(\uparrow)$ levels. Importantly, the sign of the dichroism signals are the same for excitations into these oppositely polarized states. The sign at the L_3 edge for both $3d(\downarrow)$ and $s(\uparrow)$ excitations is negative and the sign at the L_2 edge is positive for both excitations. Spin-orbit coupling in the d levels affects the value of R_M,[7] but not the signs of the XMCD spectra at either the L_3 or L_2 peak for Fe, Co, and Ni. Since there is no spin-orbit coupling in the s levels we expect $R_M = -1$ for XMCD from the diffuse-magnetic moments. Based on a comparison of radial matrix elements, which have not been included in the values of A, C, and D, the relative magnitude of the diffuse XMCD should be small compared to the $3d$ XMCD.

We identify the negative Co and Ni XMCD intensities between the shoulders B and the L_2 edge as being due to diffuse magnetic moments. The effects of diffuse magnetism are not present in the Fe XMCD spectra. They may

TABLE II. XMCD intensities at the L_2 and L_3 edges for excitation into spin polarized $s(\uparrow)$ and $3d(\downarrow)$ levels and their ratio $R_M = \Delta A_{L_3}/\Delta A_{L_2}$.

	ΔA_{L_3}	ΔA_{L_2}	R_M
s XMCD	$-2/3D$	$2/3D$	-1
$3d$ XMCD	$-2/3A + 2/3C$	$2/3A - 2/3C$	-1

be obscured by the presence of the positive going shoulder on the L_3 peak or the relative magnitude of the diffuse moment may be too low to be observed, see Table I. In Fig. 7 we show the XMCD signal due to diffuse magnetism for both Ni and Co determined from a simple model. To model the diffuse XMCD we have used a step-function line shape, which reflects a broad s-band with nearly constant density of state. We have assumed that $R_M=-1$ so that the diffuse-XMCD signal goes to zero above the L_2 edge. While the XMCD line shape due to diffuse magnetic moments is undoubtably more complicated, this simple model serves to illustrate the importance of considering diffuse magnetism in XMCD.

V. DICHROISM SUM RULES

In this section we use high-quality experimental spectra to test the application of the dichroism sum rules to solids. The samples used were bcc Fe, fcc Co, and fcc Ni thin films grown on Cu(001), Figs. 6 and 7. The Ni and Co films were magnetized along their easy axis which is in-plane for the Co film ($\langle 110\rangle$ direction) and perpendicular to the surface for the Ni film. The Fe film was magnetized in-plane in the $\langle 110\rangle$ direction, which is 35.3 degrees from the easy axis of bcc Fe, $\langle 100\rangle$.[29]

From Thole *et al.*[13] and Carra *et al.*[14] the orbital moment per hole can be determined from

$$\frac{\Delta A_{L_3}+\Delta A_{L_2}}{A_t}=\frac{\int_{L_3}\sigma_M(\hbar\omega)d\omega+\int_{L_2}\sigma_M(\hbar\omega)d\omega}{\int_{L_{2,3}}[\sigma_0(\hbar\omega)+\sigma_+(\hbar\omega)+\sigma_-(\hbar\omega)]d\omega}=\frac{\langle L_z\rangle}{2n_h} \tag{8}$$

for excitation into d orbitals, where n_h is the number of valence d holes and the integrations are over the entire L_2, L_3, or $L_{2,3}$ edge. Similarly, from Carra *et al.*[14]

$$\frac{\Delta A_{L_3}-2\Delta A_{L_2}}{A_t}=\frac{\int_{L_3}\sigma_M(\hbar\omega)d\omega-2\int_{L_2}\sigma_M(\hbar\omega)d\omega}{\int_{L_{2,3}}[\sigma_0(\hbar\omega)+\sigma_+(\hbar\omega)+\sigma_-(\hbar\omega)]d\omega}=\frac{2}{3n_h}\langle S_Z\rangle+\frac{7}{3n_h}\langle T_Z\rangle\ , \tag{9}$$

where $\langle T_Z\rangle$ is the magnetic dipole term. Both these equations are derived for atoms, so they ignore band-structure effects and transitions into s orbitals. This makes their application to solids difficult since σ_+, σ_-, σ_0, and to a lesser extend σ_M each contain excitations into levels not included in the calculation. For example, XMCD due to diffuse magnetic moments is not accounted for in these equations. Also, the number of valence holes, n_h, is not precisely known. The degree of polarization used for the measurements must be well known since this affects the values of ΔA_{L_3} and ΔA_{L_2}. Another source for uncertainty is the separation of ΔA_{L_3} and ΔA_{L_2}. Finally, the sample magnetization must be saturated for the sum-rule results to be meaningful. We have chosen samples which exhibit near 100% remanence to minimize this uncertainty.

Noting the difficulties discussed above in applying the dichroism sum rules, we test them in the following manner. First, we subtract the dichroism due to diffuse magnetic moments from the Ni and Co spectra. The values of ΔA_{L_3} and ΔA_{L_2} obtained from these spectra are then adjusted for incomplete photon polarization and nonparallel alignment of Σ and $\mathbf{M}$. For n_h we use the theoretical values of 3.1 for Fe, 2.1 for Co, and 1.0 for Ni.[30] To obtain A_t we assume $\sigma_0=1/2(\sigma_++\sigma_-)$ and a step-function continuum background spectra with a 2:1 L_3/L_2 intensity ratio. We also assume that $\langle T_Z\rangle$ is negligible since the Fe, Co, and Ni atoms in these thin films are in a cubic environment.[14] The absolute values of $\langle S_Z\rangle$ and $\langle L_Z\rangle$ obtained in this manner are compared to values determined by neutron diffraction[18] for bcc Fe, hcp Co, and fcc Ni in Fig. 8. These neutron-diffraction values are in agreement with calculations,[31] which also give theoretical values of $\langle L_Z\rangle=0.12$ and $\langle S_Z\rangle=0.8$ for fcc Co.

We have also determined $\langle L_Z\rangle$ and $\langle S_Z\rangle$ for Co and

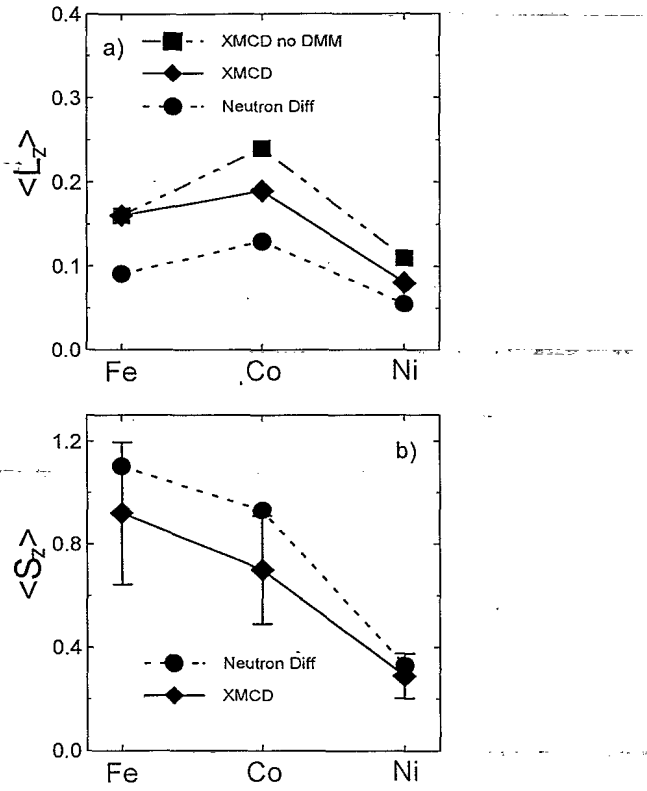

FIG. 8. (a) Values of $\langle L_Z\rangle$ obtained using (8) compared to values obtained by neutron diffraction (Ref. 18). The XMCD values include large uncertainties, ±30%, but show the same trend as the neutron diffraction values. Not accounting for dichroism due to diffuse magnetic moments (DMM) has a large effect on $\langle L_Z\rangle$ values for Ni and Co. Error bars have been omitted for clarity. (b) Values of $\langle S_Z\rangle$ obtained using (9) compared to values obtained by neutron diffraction (Ref. 18). The XMCD values show the same trend as the neutron-diffraction values. Not accounting for dichroism due to diffuse magnetic moments has a negligible effect on $\langle S_Z\rangle$ values for Ni and Co.

Ni without correcting for diffuse magnetic moments. To do this we use a photon energy just below the onset of the L_2 peaks to define the separation of ΔA_{L_3} and ΔA_{L_2}. If the Co and Ni spectra are not corrected for diffuse magnetic moments the values of $\langle S_Z \rangle$ are changed by less than 2%, while values of $\langle L_Z \rangle$ are 25% larger for Co and 40% larger for Ni (see Fig. 8). Including diffuse magnetic moments has a large effect on the $\langle L_Z \rangle$ sum rule, but has little effect on the $\langle S_Z \rangle$ the sum rule. This shows that subtleties in the interpretation of dichroism spectra can greatly influence the application of the $\langle L_Z \rangle$ sum rule.

We estimate the error in our values of $\langle L_Z \rangle$ and $\langle S_Z \rangle$ obtained by (8) and (9) to be quite large, perhaps 30%, due primarily to the uncertainties in n_h and A_t. With this large of an uncertainty it is difficult to obtain quantitative information from (8) and (9). However, the values of both $\langle S_Z \rangle$ and $\langle L_Z \rangle$ for Fe, Co, and Ni determined from the XMCD spectra have the same trend as values determined by neutron diffraction, Fig. 8. This is true whether or not diffuse magnetic moments are considered. If diffuse magnetic moments are considered the values of $\langle L_Z \rangle$ determined from (8) are each a factor of $\sim 1.6 \pm 0.2$ times the neutron-diffraction results, while the values of $\langle S_Z \rangle$ determined from (9) are each a factor of $\sim 0.8 \pm 0.08$ times the neutron-diffraction values. If diffuse magnetic moments are not considered the values of $\langle L_Z \rangle$ determined from (8) are each a factor of $\sim 1.9 \pm 0.2$ times the neutron-diffraction results. There may be a systematic error in our measurement of A_t, in the values of n_h or in our calculation of the degree of polarization which is responsible for this observed proportionality. The comparisons in Fig. 8 show that both the $\langle S_Z \rangle$ and $\langle L_Z \rangle$ dichroism sum rules are qualitatively accurate for Fe, Co, and Ni.

Based on their qualitative accuracy, we feel that the dichroism sum rules can be best applied to measured changes in $\langle S_Z \rangle$ and $\langle L_Z \rangle$ for a specific element in different environments. If the dichroism spectra are obtained and analyzed in a consistent manner, uncertainties due to n_h, A_t, the degree of polarization, and the separation of ΔA_{L_3} and ΔA_{L_2}, will cancel. Since errors due to saturation can be greater than the actual changes being measured, the method of measuring absorption must be well understood in order to eliminate experimental artifacts. Under these conditions, changes in the dichroism spectra can be interpreted as changes in either $\langle S_Z \rangle$ or $\langle L_Z \rangle$.

VI. SUMMARY AND CONCLUSIONS

X-ray magnetic circular dichroism in the $L_{2,3}$ absorption spectra of thin films has been investigated by total electron yield. The total electron yield method of measuring absorption was studied in great detail, using samples of known thickness, angular-dependent dichroism measurements, and model calculations. These results show that errors due to saturation in the total electron yield measurement can be kept to less than 5% if proper experimental conditions are used. The proper experimental conditions may be determined by model calculations. For thick Fe films, a photon angle of incidence less than 50° is required if the degree of circular polarization is 0.85.

High-quality Fe, Co, and Ni XMCD spectra were used to test the $\langle L_Z \rangle$ and $\langle S_Z \rangle$ dichroism sum rules. The resulting values of $\langle L_Z \rangle$ and $\langle S_Z \rangle$ for Fe, Co, and Ni include large uncertainties, making the quantitative application of the sum rules difficult. One possible source of uncertainty is dichroism due to diffuse magnetic moments. We have developed a simple model which accounts for the effects of diffuse magnetic moments in the XMCD spectra of Co and Ni. This has a large effect on values of $\langle L_Z \rangle$ showing the importance of properly considering XMCD features not associated with $3d$ levels. While the values of $\langle S_Z \rangle$ and $\langle L_Z \rangle$ for Fe, Co, and Ni determined from the XMCD spectra include large uncertainties, they are found to be proportional to values determined by neutron diffraction. This suggests that changes in $\langle L_Z \rangle$ and $\langle S_Z \rangle$ can be measured using XMCD. To do this, experimental artifacts such as saturation must be understood and accounted for. We feel that the applicability of the sum rules will be restricted to measuring relative changes in $\langle L_Z \rangle$, $\langle S_Z \rangle$ or $\langle L_Z \rangle / \langle S_Z \rangle$ for specific atoms in different environments. This is, in itself, an area of considerable interest and importance.

ACKNOWLEDGMENTS

This work was supported by the National Science Foundation, Division of Materials Research under Grant No. DMR-91-15987. The Synchrotron Radiation Center is a national facility supported by the NSF Division of Materials Research.

[1]C. T. Chen, F. Sette, Y. Ma, and S. Modesti, Phys. Rev. B **42**, 7262 (1990).
[2]G. R. Harp, S. S. P. Parkin, W. L. O'Brien, and B. P. Tonner, J. Appl. Phys. (to be published).
[3]W. L. O'Brien, B. P. Tonner, G. R. Harp, and S. S. P. Parkin, J. Appl. Phys. (to be published).
[4]Y. U. Idzerda, L. H. Tjeng, H. J. Lin, C. J. Gutierrez, G. Meigs, and C. T. Chen, Phys. Rev. B **48**, 4144 (1993).
[5]W. L. O'Brien, J. Zhang, and B. P. Tonner, J. Phys. Condens. Matter **5**, L515 (1993).
[6]W. L. O'Brien and B. P. Tonner (unpublished).
[7]N. V. Smith, C. T. Chen, F. Sette, and L. F. Mattheiss, Phys. Rev. B **46**, 1023 (1992).
[8]W. L. O'Brien and B. P. Tonner, Phys. Rev. **50**, 2963 (1994).
[9]Y. Wu, J. Stöhr, B. D. Hermsmeir, M. G. Samant, and D. Weller, Phys. Rev. Lett. **69**, 2307 (1992).
[10]W. L. O'Brien and B. P. Tonner, Phys. Rev. B **49**, 15 370 (1994).

[11]C. T. Chen, N. V. Smith, and F. Sette, Phys. Rev. B **43**, 6785 (1991).
[12]M. G. Samant, J. Stöhr, S. S. P. Parkin, G. A. Held, B. D. Hermsmeier, F. Herman, M. van Schilfgaarde, L. C.-Duda, D. C. Mancini, N. Wassdahl, and R. Nakajima, Phys. Rev. Lett. **72**, 1112 (1994).
[13]B. T. Thole, Paolo Carra, F. Sette, and G. van der Laan, Phys. Rev. Lett. **68**, 1943 (1992).
[14]P. Carra, B. T. Thole, M. Altarelli, and X. Wang, Phys. Rev. Lett. **70**, 694 (1993).
[15]J. L. Erskine and E. A. Stern, Phys. Rev. B **12**, 5016 (1975).
[16]R. Wu, D. Wang, and A. J. Freeman, Phys. Rev. Lett. **71**, 3581 (1993).
[17]R. Wu, D. Wang, and A. J. Freeman (unpublished).
[18]M. B. Stearns, in *Numerical Data and Functional Relationships in Science and Technology,* edited by H. P. J. Wijn, Landolt-Börnstein, New Series, Group 3, Vol. 19, Pt. a (Springer-Verlag, Berlin, 1986); D. Bonnenberg, K. A. Hempel, and H. P. J. Wijn, *ibid.*
[19]O. Eriksson, A. M. Boring, R. C. Albers, G. W. Fernando, and B. R. Cooper, Phys. Rev. B **45**, 2868 (1992).
[20]J. Vogel and M. Sacchi, Phys. Rev. B **49**, 3230 (1994).
[21]R. W. C. Hansen, W. L. O'Brien, and B. P. Tonner (unpublished).
[22]J. J. Yeh and I. Lindau, At. Data Nucl. Data Tables **32**, 2 (1985).
[23]H. Li and B. P. Tonner, Phys. Rev. B **40**, 10241 (1989).
[24]P. Strange, P. J. Durham, and B. L. Gyorffy, Phys. Rev. Lett. **67**, 3590 (1991).
[25]L. H. Tjeng, C. T. Chen, P. Rudolf, G. Meigs, G van der Laan, and B. T. Thole, Phys. Rev. B **48**, 13 378 (1993).
[26]T. Jo and G. Sawatzky, Phys. Rev. B **43**, 8771 (1991).
[27]G. van der Laan and B. T. Thole, Phys. Rev. B **43**, 13 401 (1991).
[28]H. Bethe and E. Salpeter, *Qauntum Mechanics of One- and Two-Electron Atoms* (Springer-Verlag, New York, 1957).
[29]K. Kalki, D. D. Chambliss, K. E. Johnson, R. J. Wilson, and S. Chiang, Phys. Rev. B **48**, 18 344 (1993).
[30]D. A. Papaconstantopoulos, *Handbook of the Band Structure of Elemental Solids* (Plenum. New York, 1986).
[31]P. Soderlind, O. Eriksson, B. Johansson, R. C. Albers, and A. M. Boring, Phys. Rev. B **45**, 12 911 (1992).